Androgen receptor–negative human prostate cancer cells induce osteogenesis in mice through FGF9-mediated mechanisms

Zhi Gang Li,[1] Paul Mathew,[1] Jun Yang,[1] Michael W. Starbuck,[1] Amado J. Zurita,[1] Jie Liu,[1] Charles Sikes,[1] Asha S. Multani,[2] Eleni Efstathiou,[1] Adriana Lopez,[3] Jing Wang,[4] Tina V. Fanning,[5] Victor G. Prieto,[5] Vikas Kundra,[6] Elba S. Vazquez,[7] Patricia Troncoso,[5] Austin K. Raymond,[5] Christopher J. Logothetis,[1] Sue-Hwa Lin,[8] Sankar Maity,[9] and Nora M. Navone[1]

[1]Department of Genitourinary Medical Oncology, [2]Department of Cancer Genetics, [3]Department of Biostatistics, [4]Department of Bioinformatics and Computational Biology, [5]Department of Pathology, and [6]Department of Diagnostic Radiology, The University of Texas MD Anderson Cancer Center, Houston, Texas, USA. [7]Department of Biological Chemistry, School of Sciences, University of Buenos Aires, and Consejo Nacional de Investigaciones Científicas y Técnicas, Buenos Aires, Argentina. [8]Department of Molecular Pathology and [9]Department of Molecular Genetics, The University of Texas MD Anderson Cancer Center, Houston, Texas, USA.

In prostate cancer, androgen blockade strategies are commonly used to treat osteoblastic bone metastases. However, responses to these therapies are typically brief, and the mechanism underlying androgen-independent progression is not clear. Here, we established what we believe to be the first human androgen receptor–negative prostate cancer xenografts whose cells induced an osteoblastic reaction in bone and in the subcutis of immunodeficient mice. Accordingly, these cells grew in castrated as well as intact male mice. We identified FGF9 as being overexpressed in the xenografts relative to other bone-derived prostate cancer cells and discovered that FGF9 induced osteoblast proliferation and new bone formation in a bone organ assay. Mice treated with FGF9-neutralizing antibody developed smaller bone tumors and reduced bone formation. Finally, we found positive FGF9 immunostaining in prostate cancer cells in 24 of 56 primary tumors derived from human organ-confined prostate cancer and in 25 of 25 bone metastasis cases studied. Collectively, these results suggest that FGF9 contributes to prostate cancer–induced new bone formation and may participate in the osteoblastic progression of prostate cancer in bone. Androgen receptor–null cells may contribute to the castration-resistant osteoblastic progression of prostate cancer cells in bone and provide a preclinical model for studying therapies that target these cells.

Introduction

Prostate cancer is the second leading cause of cancer death among men in the United States (1). Androgen deprivation is the standard therapy for advanced prostate cancer. Although the disease in most cases initially responds, it often progresses and becomes castration resistant. At that stage, men with prostate cancer display characteristically osteoblastic bone metastases, which is the main cause of morbidity and mortality of the disease (2–5). Although the mechanism of androgen-independent progression in bone is still poorly understood, the clinical observations imply that delineating the mechanisms leading to castration-resistant progression and induction of bone growth in the metastatic lesions may be key to understanding prostate cancer bone metastases.

Several mechanisms have been implicated in the castration-resistant growth of prostate cancer. These mechanisms imply the existence of an active androgen receptor pathway in most cases. These mechanisms include: (a) androgen receptor gene amplification (6, 7); (b) changes in ligand specificity due to mutations in the ligand-binding domain of the androgen receptor (6, 7); (c) ligand-independent activation of the androgen receptor due to increased MAPK signaling (6); and (d) alteration in the balance and/or recruitment of androgen receptor coactivators and corepressors (8, 9). The role of the androgen receptor pathway in the osteoblastic progression of prostate cancer is unknown. As all available models of osteoblastic bone metastases are androgen responsive (10–13), this has led to the assumption that the osteoblastic progression of prostate cancer is dependent on the presence of an active androgen receptor pathway. In support of this hypothesis, it was reported that expression of prostate-specific antigen (PSA; the best-characterized downstream target of the androgen receptor) has been associated with the osteoblastic phenotype (14) and that PSA induces osteosarcoma cell line differentiation (15). However, whether androgen receptor is required for prostate cancer cells to induce new bone formation and how the induction of new bone may affect the growth and/or survival of prostate cancer cells in bone are not completely understood, in part because few of the available models recapitulate the prostate cancer–bone interaction.

In an effort to meet the need for additional clinically relevant models of prostate cancer bone metastasis, we and others at our institution developed a strategy to harvest prostate cancer tissue specimens from bone metastases and use them to generate murine models of prostate cancer (16, 17). We previously used this strategy to establish 2 bone-derived prostate cancer cell lines, MDA PCa (MD Anderson prostate cancer) 2a and MDA PCa 2b (16). We now report the development of 2 prostate cancer xenografts, MDA PCa 118a and MDA PCa 118b, from bone metastases

Nonstandard abbreviations used: BMP, bone morphogenetic protein; DKK1, dickkopf-1; FGFR, FGF receptor; MDA PCa, MD Anderson prostate cancer; PSA, prostate-specific antigen; PTHrP, parathyroid hormone–related peptide; TRAP, tartrate-resistant acid phosphatase.

Conflict of interest: The authors have declared that no conflict of interest exists.

Citation for this article: *J. Clin. Invest.* **118**:2697–2710 (2008). doi:10.1172/JCI33093.

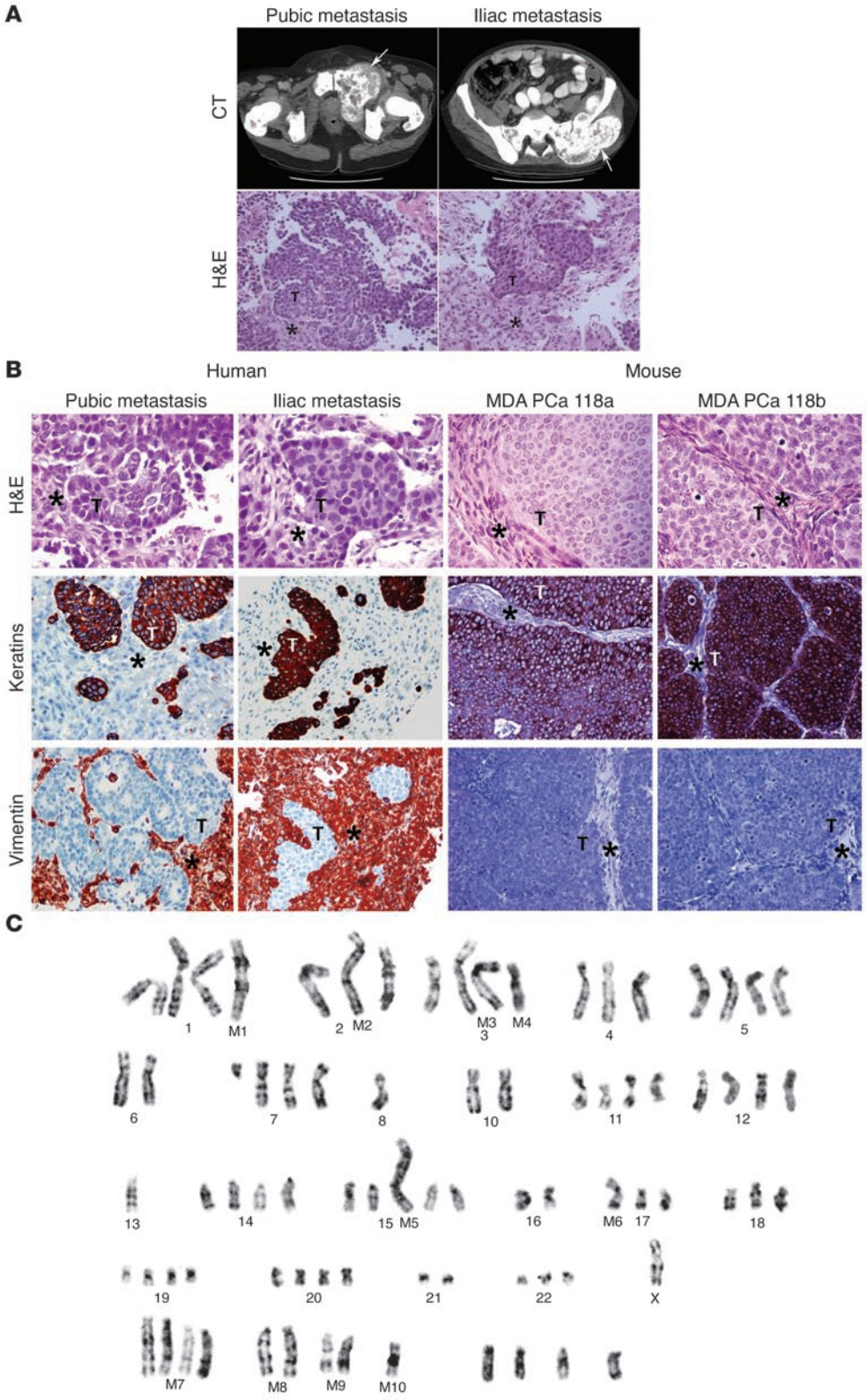

Figure 1
The origin of MDA PCa 118 xenografts; histopathologic and immunohistochemical stains of human tissue biopsy specimens and the derived MDA PCa 118 variant; and the karyotype of MDA PCa 118b cells. (**A**) Top: Contrast-enhanced CT scans of the pelvis of a 49-year-old man of mixed European descent with androgen-independent prostate cancer show the expansile ossified lesion involving the left pubis (arrow, left panel) that was the source of MDA PCa 18a cells and the left ilium (arrow, right panel) that was the source of the MDA PCa 118b cells. Bottom: H&E-stained tissue sections of biopsy specimens from the lesions in the pubic (arrow, top left panel) and iliac (arrow, top right panel) metastases. Original magnification, ×200. T, prostate cancer cells; asterisks indicate stroma. (**B**) Top row: H&E-stained biopsy specimens of the pubic and iliac metastases and the MDA PCa 118a and 118b variants. Middle row: Cytokeratin-stained sections. Bottom row: Vimentin-stained sections. The mouse stroma in the xenografts did not stain for vimentin because the Ab (clone V9) reacts with human, not mouse, vimentin. Original magnification, ×200. T, prostate cancer cells; asterisks indicate stroma. (**C**) Giemsa-banded karyotype of MDA PCa 118b human prostate cancer cells showing marker chromosomes (M1–M10) and various anomalies. The tentative identification of the markers is as follows: M1, iso(1p); M2, t(3q;6p); M3, t(3q;?); M4, del(3p); M5, 15p+; M6, 17p+; M7 and M8, markers containing an abnormally banded region (ABR); M9, t(11q;18q); M10, unidentified marker.

in a man with castration-resistant prostate cancer. These new tumor lines induced robust osteoblastic reactions in the bone and subcutis of immunodeficient mice. In this report, we present the initial characterization of this model and show that the osteoblastic reaction can be induced in the absence of androgen receptor expression. In addition, we identify a paracrine factor that is likely to be involved in the interactions between prostate cancer cells and bone that lead to the formation of bone.

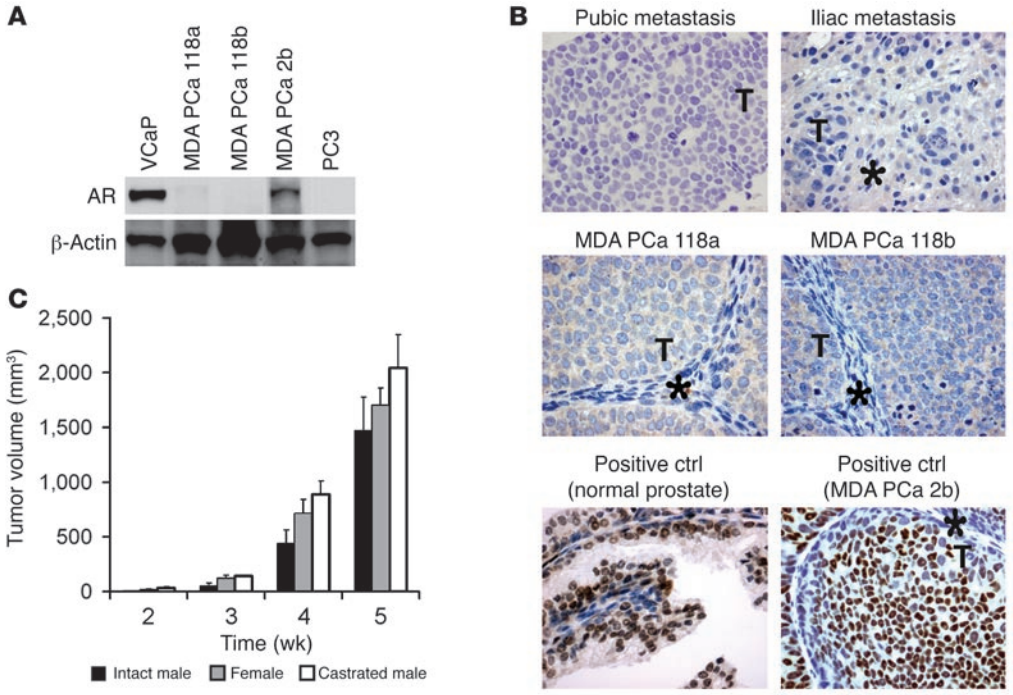

Figure 2

Androgen receptor expression in the human tissue biopsy samples and MDA PCa 118 variants and the in vivo growth of MDA PCa 118b cells in sham-operated male, female, or castrated male mice. (**A**) Western blot of androgen receptor (AR) expression in the MDA PCa 118a and MDA PCa 118b prostate cancer xenografts probed with mAb against human androgen receptor. Positive controls were the human prostate cancer cell lines VCaP and MDA PCa 2b, and the negative control was the human prostate cancer cell line PC3. β-Actin was used as a loading control. (**B**) Immunohistochemical staining of biopsy samples from the pubic metastasis (the source of MDA PCa 118a) and iliac metastasis (source of MDA PCa 118b) and of the MDA PCa 118a and MDA PCa 118b xenografts with an Ab against human androgen receptor. Normal prostate and MDA PCa 2b cells grown subcutaneously in SCID mice were used as positive controls (ctrl). Original magnification, ×200. (**C**) Volume of tumors formed 2–5 weeks after subcutaneous injection of MDA PCa 118b cells in sham-operated (intact) male, female, and castrated male mice (5 per group). Tumor volumes (in mm^3) were calculated using the formula for volume of an ellipsoid [$4/3\pi$ (length/2 × width/2 × height/2)]. Error bars indicate SEM.

Results

Generation of MDA PCa 118a and 118b xenografts from prostate cancer bone metastases. Of 17 bone tissue specimens obtained from men with prostate cancer bone metastases and implanted subcutaneously in SCID mice, only 2 led to tumor development — tumors we called MDA PCa 118a and MDA PCa 118b. These xenografts were derived from bone metastases in a 49-year-old man of mixed European descent with androgen-independent prostate cancer. MDA PCa 118a cells came from a specimen obtained from the left superior pubic ramus and MDA PCa 118b cells from the sacroiliac zone of an exophytic lesion in the left hemipelvis (Figure 1A). These tissue specimens were obtained by needle biopsy. At the time of the biopsy, the patient's serum PSA was 87 ng/ml, and he had widespread osteoblastic metastases. Histological analysis of the biopsy tissue from the left pubic and iliac lesions confirmed the presence of high-grade adenocarcinoma (Figure 1A). The tumor histology was similar in both sites, with evidence of both epithelial differentiation and focal areas of spindle cell differentiation. The dominant cytological/histological appearance was that of epithelioid tumor cells in sheets and in small groups, with a suggestion of primitive gland formation. Individual cells had small to intermediate amounts of cytoplasm and round to oval nuclei containing variably prominent nucleoli (Figure 1A). These features are consistent with metastases from a high-grade prostate adenocarcinoma.

Subcutaneous implantation of pieces of these metastatic tumors in male SCID mice led to tumor development, but the tumor cells derived from those xenografts did not survive in culture. As a result, we have maintained the xenografts by passage in SCID mice. To date, the tumor line has been maintained for 3 years, with passage every 60 days. Samples of these xenografts frozen in DMSO at different passages are able to regrow in SCID mice after being thawed.

MDA PCa 118 tumor is high-grade adenocarcinoma that expresses cytokeratins. To further characterize these new xenografts, we compared the histopathology of the MDA PCa 118 variants with that of their human tumors of origin as well as the expression of markers of epithelium (cytokeratins), mesenchyme (vimentin), and neuroendocrine differentiation (synaptophysin and chromogranin A) by immunohistochemical staining. MDA PCa 118 xenografts were high-grade adenocarcinoma but had glandular structures that were less apparent than in the human tumor of origin (Figure 1B). The neoplastic cells of both the MDA PCa 118 variants and those of the human tumor of origin expressed cytokeratins. The human-specific anti-vimentin Ab that we used (clone V9) reacted only with stroma cells in the human tumor of origin. The observation that this anti-vimentin Ab did not react with stroma cells in the MDA PCa 118 xenografts (Figure 1B) indicated that human stroma cells were not propagated in the MDA PCa 118 xenografts. Neither the MDA PCa 118 variants nor the human tumor of origin expressed chromo-

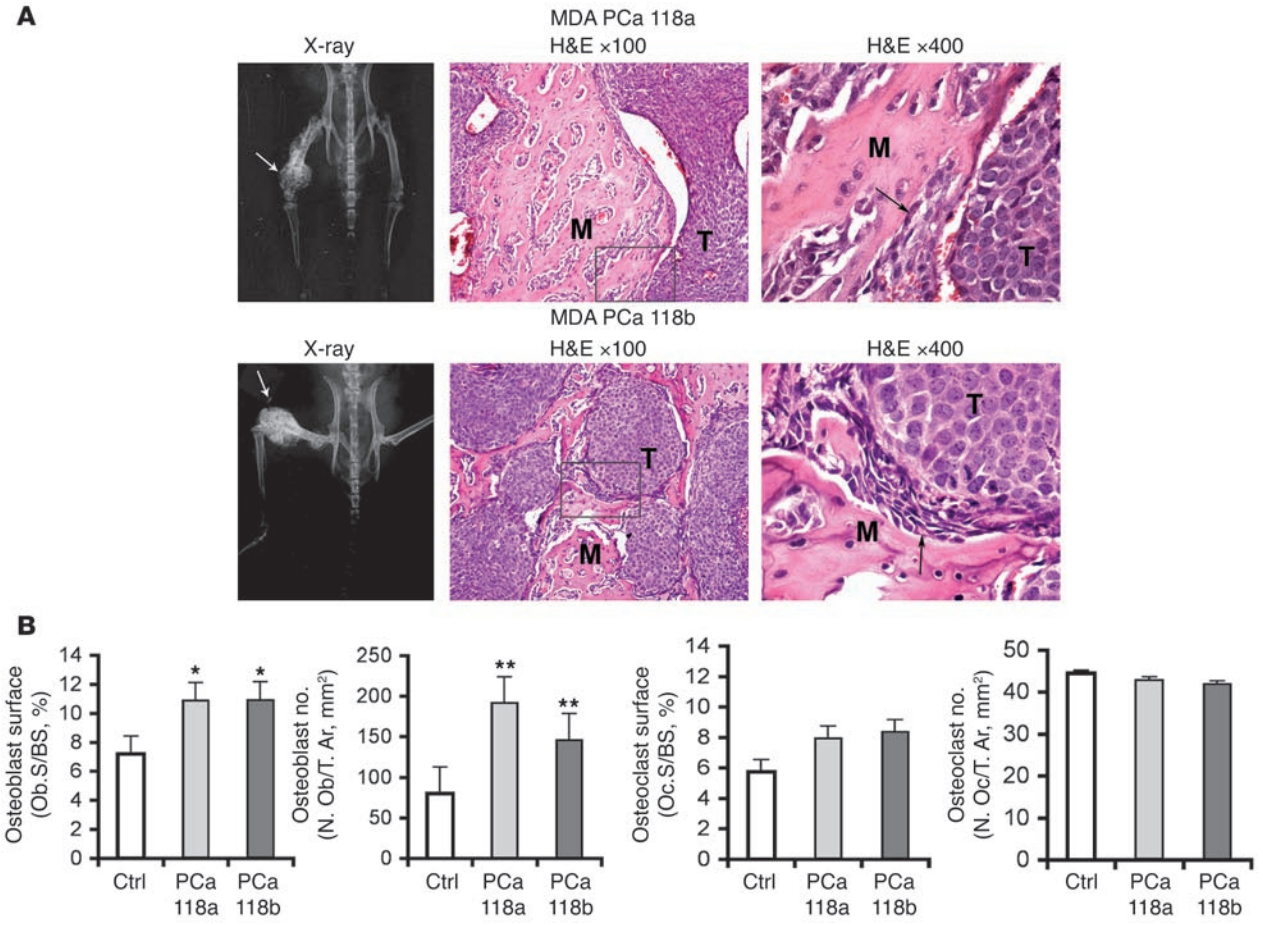

Figure 3

MDA PCa 118 variants growing in bones of immunodeficient mice. (**A**) Radiographs at left show mouse pelvis and rear limbs 9 weeks after intrafemoral implantation of MDA PCa 118a (top) and MDA PCa 118b cells (bottom). Arrows indicate increased density in bone and exophytic lesions resembling the human sample of origin. The middle and right panels show H&E-stained sections of lesions induced by the intrafemoral implantation of MDA PCa 118a and MDA PCa 118b cells into intact male SCID mice. M, bone matrix; arrows indicate osteoblasts. Right panels show higher magnification of the areas indicated by boxes in the middle panels. (**B**) Osteoblast- and osteoclast-associated parameters quantified with the OsteoMeasure system (OsteoMetrics). Ob(Oc).S/BS, osteoblast (osteoclast) surface as a percentage of bone surface; N. Ob(Oc)/T. Ar, number of osteoblasts (osteoclasts) per area of tissue. Error bars indicate SEM. $^{*}P < 0.05$; $^{**}P < 0.0125$.

granin A or synaptophysin (data not shown). These results demonstrated that MDA PCa 118 xenografts, like the human tumor of origin, are adenocarcinomas positive for cytokeratin expression and have not undergone neuroendocrine differentiation.

Karyotype analysis of MDA PCa 118b xenografts. To identify numerical and structural chromosome abnormalities as well as marker chromosomes associated with this new model, we performed detailed karyotype analysis. The tumor lines we used for karyotyping had grown in SCID mice for 3 years. The chromosome number in this cell line ranged from 55 to 80, with the modal chromosome number being 64. Ten consistent clonal markers, M1–M10 chromosomes, were present in this cell line. The tentative identification of the markers is as follows: M1, iso(1p); M2, t(3q;6p); M3, t(3q;?); M4, del(3p); M5, 15p+; M6, 17p+; M7 and M8, markers containing abnormally banded region (ABR); M9, t(11q;18q); M10, unidentified marker. A karyotype showing marker chromosomes and other anomalies is shown in Figure 1C. Two populations of cells were present in this cell line. One had all 10 markers (M1–M10; Figure 1C), whereas the other had only markers M7–M10 (not shown).

MDA PCa 118 xenografts do not express the androgen receptor and grow in castrated mice. Because the patient from whom the MDA PCa 118 xenografts were generated had significant amounts of serum PSA at the time of biopsy, we expected the xenografts to express androgen receptor. However, Western blotting showed that neither xenograft expressed the androgen receptor (Figure 2A), and no PSA could be detected in the blood of tumor-bearing mice (data not shown). Accordingly, immunohistochemical staining of the xenografts was negative for androgen receptor expression (Figure 2B). Also, tumor cells in the human biopsy specimens used to generate the xenografts did not express androgen receptor (Figure 2B), PSA, or prostate-specific alkaline phosphatase (data not shown). The discrepancy between serum PSA levels and tissue PSA expression probably resulted from heterogeneity within the prostate tumor, which can occur both within and between patients (18).

Next, we tested the tumorigenicity of MDA PCa 118b cells on their subcutaneous implantation in surgically castrated male mice (16), in female mice, and in sham-operated male mice (Figure 2C). The MDA PCa 118b cells produced tumors in all mice injected (5

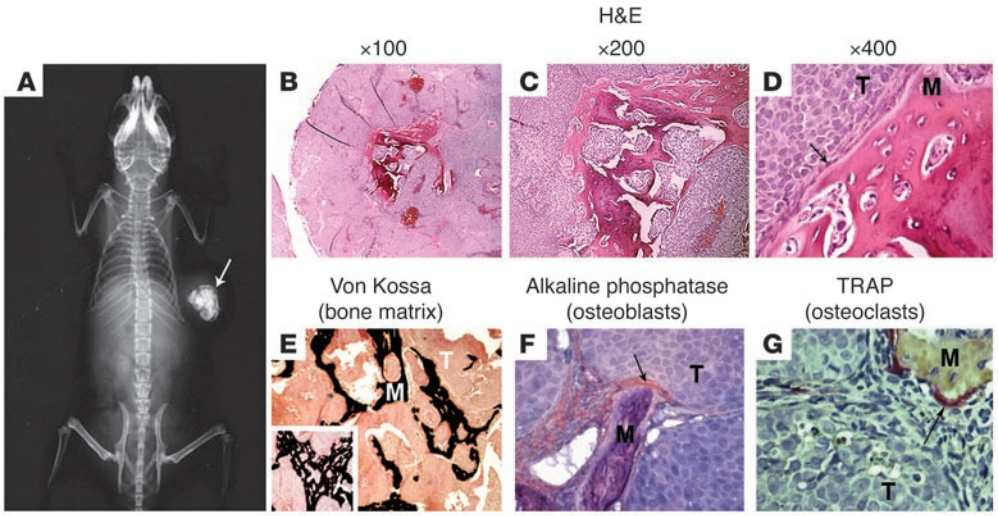

Figure 4
MDA PCa 118b xenograft growing subcutaneously in immunodeficient mice. (**A**) Whole-body radiograph of mouse with subcutaneous MDA PCa 118b implant indicates bone-like increase in density in the tumor area (arrow). (**B**–**G**) Histologic analyses of MDA PCa 118b cells growing subcutaneously. (**B**–**D**) Representative areas of MDA PCa 118b xenograft with bone-like extracellular matrix (H&E stain; original magnifications, ×100, ×200, and ×400). Arrow indicate osteoblasts. (**E**) Positive von Kossa staining (black) indicates calcified matrix in the MDA PCa 118b xenograft. Original magnification, ×100; inset original magnification, ×400. (**F**) Positive alkaline phosphatase (red) staining in bone lining cells indicates osteoblasts (arrow). Original magnification, ×400. (**G**) TRAP (red) staining indicates osteoclasts (arrow). Original magnification, ×400.

mice per group). No statistically significant difference in tumor size was found between the groups. These findings suggested that MDA PCa 118 xenografts can sustain androgen-independent growth.

MDA PCa 118a and 118b xenografts induce robust osteoblastic reactions upon femoral implantation in SCID mice. Because the xenografts were generated from prostate cancer specimens from osteoblastic bone lesions, we next tested whether they could produce similar lesions on their implantation into the bones of intact male SCID mice. We found that the MDA PCa 118a and MDA PCa 118b cells induced robust osteoblastic reactions in the bones of all injected mice 9 weeks after intrafemoral injection (Figure 3). None of the contralateral legs of any injected mouse showed evidence of osteoblastic lesions. Histopathologic analysis of the tumors developed by both MDA PCa 118 variants showed tumor cells surrounded by bone matrix (Figure 3), with osteoblasts visible in the bone near the injected cells (Figure 3). Histomorphometric analysis of the MDA PCa 118a and 118b cells growing in bone demonstrated an increased number of osteoblasts but not osteoclasts when compared with the contralateral normal femur (Figure 3). Collectively, these results suggested that MDA PCa 118 cells induce the formation of new bone on their injection into the bones of immunodeficient mice.

Subcutaneous MDA PCa 118 xenografts form bone-like matrix with marrow elements in SCID mice. During passage of the xenografts in SCID mice, we noticed on slicing that the subcutaneous tumors seemed gritty. X-ray imaging of the mice with the subcutaneous MDA PCa 118b implants showed areas of high density within the xenografts (Figure 4A). Histopathologic and immunohistochemical analysis indicated the formation of a bone-like extracellular matrix, with cellular elements typical of bone (e.g., osteoblasts, osteoclasts) (Figure 4, B–G). The presence of calcified matrix was verified by von Kossa staining (of undecalcified tumor specimens embedded in methylmethacrylate; Figure 4E) and the presence of osteoblasts in the bone-tumor interface by alkaline phosphatase staining (Figure 4F). Multinucleated, tartrate-resistant acid phosphatase–positive (TRAP-positive) cells in the bone-tumor interface were considered osteoclasts (Figure 4G). Similar results were obtained from the MDA PCa 118a xenografts (data not shown). These findings demonstrated that MDA PCa 118 tumors induced ectopic bone formation in the subcutis of male SCID mice.

Stromal cells in the ectopic bone matrix are mouse derived. The ectopic bone-like matrix that formed in the subcutaneous MDA PCa 118a and 118b tumors was accompanied by osteoblasts and osteoclasts. We sought to determine whether these stromal cells arose from mouse-derived mesenchyme progenitors, from mesenchymal cells present in the biopsy material from the patient, or by an epithelial-mesenchymal transition of the human prostate cancer cells. First, we used FISH with a mouse Y chromosome probe and human centromere probes to determine whether the stromal cells were of mouse or human origin. We found red dot staining (indicating mouse) in the cells of the bone-like matrix areas and green dot staining (indicating human) in the tumor cells (Figure 5, A and B). Red dot staining in osteocytes is shown in Supplemental Figure 1 (supplemental material available online with this article; doi:10.1172/JCI33093DS1). Diffuse green staining covering areas of stroma was autofluorescence, and bright green dots were seen only in the tumor nuclei; this can be better appreciated in the detail of the human probe (Figure 5B). To further clarify the origin of stroma cells, we used human-specific anti-mitochondria Ab and found positive staining only in areas with adenocarcinoma, with no staining in the bone-like matrix areas or stromal cells (Figure 5C). These results suggested that the stromal cells present in the bone-like tissue were of mouse origin.

MDA PCa 118 ectopic bone does not form through endochondral ossification. Bone can form in 2 ways: either directly from mesenchyme precursors (intramembranous ossification) or indirectly, when cartilage forms first and is then replaced by bone (endochondral ossification). To assess which of these mechanisms was responsible for the bone found in the subcutaneous MDA PCa 118 tumors, we performed a time-course study. MDA PCa 118b subcutaneous tumors

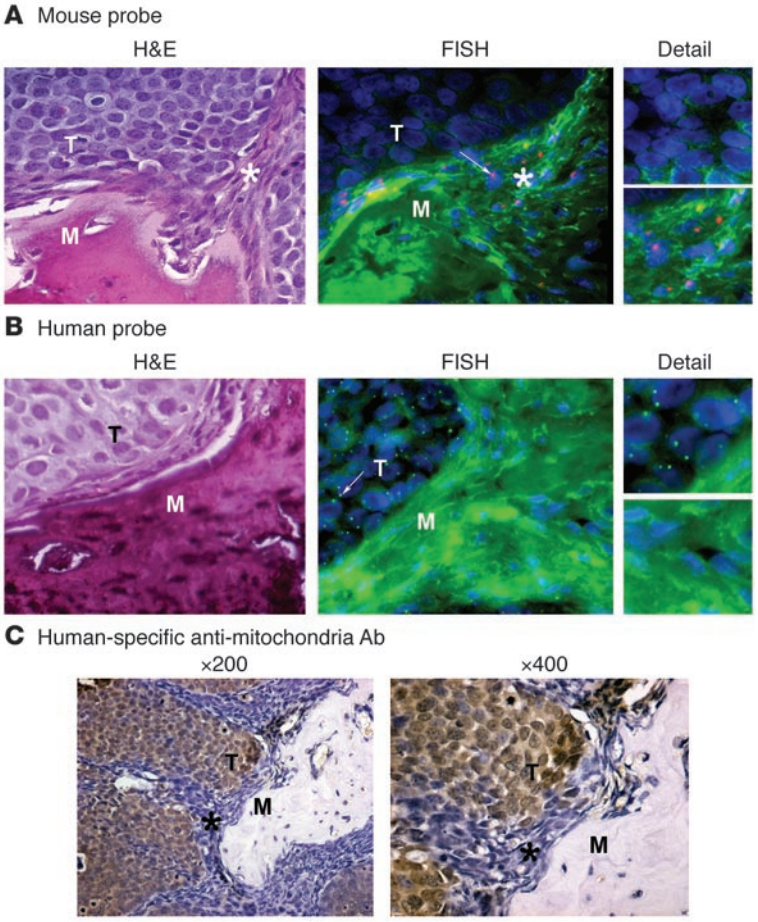

Figure 5
FISH and immunohistochemical analyses of MDA PCa 118b xenografts grown subcutaneously in SCID mice. (**A**) Photomicrographs of H&E-stained sections and FISH analyses with mouse Y chromosome paint probe (labeled with red CY3). Sections processed for FISH analysis were obtained at a distance of 15–30 μm from the H&E-stained section. Photomicrographs from FISH analysis were taken with FITC filters to visualize the tissue structure and were merged with photomicrographs of the same areas taken with a CY3 filter (to visualize the red CY3-labeled mouse chromosome) and DAPI (to visualize the blue cell nuclei). The bright red dots, seen only in the stromal area, are CY3-labeled mouse chromosome probes. Original magnification, ×630; detail, ×850. The arrow indicates the CY3-labeled mouse chromosome (red dot) that is included in the area of detail. (**B**) Photomicrographs of H&E–stained sections and FISH analysis with FITC-labeled human centromere probes for chromosome 7. Sections processed for FISH analysis were obtained at a distance of 15–30 μm from the H&E-stained section. Photomicrographs from FISH analysis were taken with FITC (to visualize the green FITC-labeled human centromere probes) and were merged with photomicrographs of same areas taken with a DAPI filter (to visualize the blue cell nuclei). The bright green dots, seen only in the tumor area, are FITC-labeled human centromere probes. Original magnification, ×630; detail, ×950. The arrow indicates the FITC-labeled human chromosome (bright green dot) that is included in the area of detail (**C**) Staining with Ab specific to human mitochondria. The areas of stroma and bone-like matrix are negative for the human antigen.

harvested at 1–4 weeks after cell injection had bone matrix–like areas that stained positively for alizarin red, a dye that detects tissue mineralization; however, we found no positive staining for Alcian blue, a dye that stains proteoglycans, suggesting that cartilage was not formed at any time during the formation of bone in the MDA PCa 118 tumors (Supplemental Figure 2). Taken together, these results suggested that MDA PCa 118–induced ectopic bone formation occurs through intramembranous osteogenesis.

MDA PCa 118 cells express bone morphogenetic proteins, Wnt ligands, dickkopf-1, and endothelin-1. Reasoning that the strong bone-forming activity of the MDA PCa 118 xenografts may reflect the production of osteogenic factors by the tumor cells, we used RT-PCR to assess the expression of bone morphogenetic protein–2 (*BMP2*), *BMP4*, *BMP6*, and *BMP7* (19–22) and members of the *WNT* family (23, 24), which are known to regulate bone formation and have been implicated in prostate cancer–induced new bone formation. cDNA prepared from PC3 and MDA PCa 2b cells (2 bone-derived prostate cancer cell lines) were included for comparison. The MDA PCa 118a and MDA PCa 118b xenografts and the PC3 cells expressed several *BMP* genes and *WNT* ligands (Figure 6A). Endothelin-1, which has been implicated in the pathogenesis of osteosclerotic bone metastases from prostate cancer (25), was expressed at roughly similar levels by all 4 cell types (Figure 6A). The MDA PCa 118a and 118b xenografts and the PC3 cells also expressed dickkopf-1 (*DKK1*), an extracellular Wnt inhibitor implicated in the pathogenesis of osteolytic lesions in patients with multiple myeloma (26, 27) and prostate cancer (23, 24) (Figure 6A). These results were confirmed using cDNA prepared from tumor cells isolated from MDA PCa 118a, MDA PCa 118b, MDA PCa 2b, and PC3 xenografts by laser-capture microdissection, suggesting that these factors are expressed by the tumor cells. These observations indicated no notable differences in the patterns of expression of putative osteoblast stimulatory factors or inhibitors by these 2 osteogenic xenografts and the osteolytic PC3 cells.

MDA PCa 118 cells express osteoclast-activating factors. We next explored the possibility that the osteogenic phenotype of the prostate cancer xenografts may result from inhibition of osteoclast activity. The presence of osteoclasts in the subcutaneous MDA PCa 118 xenografts (Figure 4G) suggested that active bone resorption occurs in parallel with bone formation in these xenografts. We thus assessed the expression of 2 osteoclast-activating factors, *RANKL* and parathyroid hormone–related peptide (*PTHRP*), that have been implicated in the pathogenesis of bone metastases (28). RT-PCR showed that MDA PCa 118 xenografts and PC3 cells, but not MDA PCa 2b cells, expressed *PTHRP* and similar, although low, amounts of *RANKL* (Figure 6A). These results were also confirmed with cDNA from laser-capture microdissected tumor cells from MDA PCa 118a, MDA PCa 118b, MDA PCa 2b, and PC3 xenografts. Finally, we found that osteoprotegerin, a natural decoy receptor for RANKL, was also expressed at similar levels in the MDA PCa 118 xenografts and PC3 cells. Thus, no substantial differences were detected in the expression of putative osteoclast regulatory factors or inhibitors between these 2 osteogenic xenografts and the osteolytic PC3 cells.

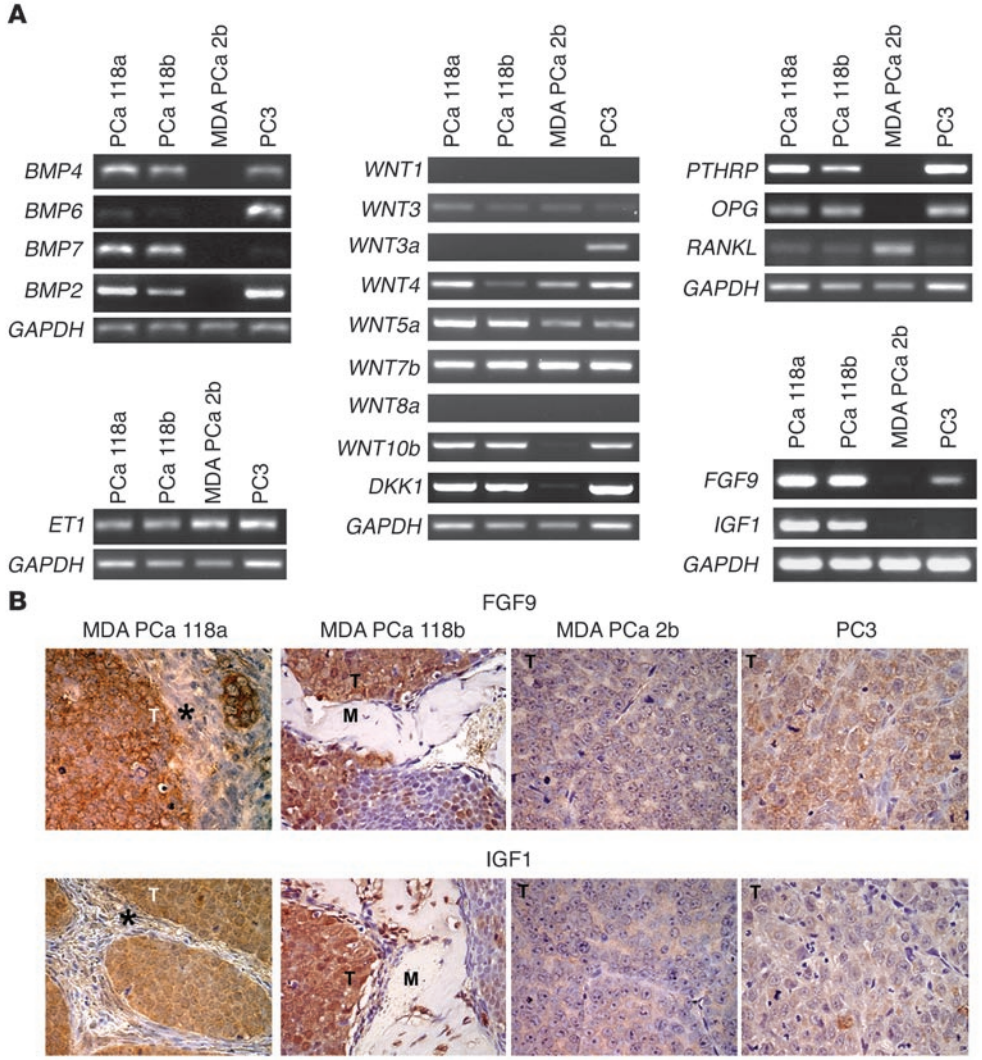

Figure 6
Gene expression patterns in prostate cancer xenografts. (**A**) RT-PCR analyses of *BMP* genes; *WNT* genes and *DKK1*; endothelin-1 (*ET1*); *PTHRP*, osteoprotegerin (*OPG*), and *RANKL*; and *IGF1* and *FGF9* in MDA PCa 118a, MDA PCa 118b, MDA PCa 2b, and PC3 prostate cancer xenograft cells. (**B**) Immunohistochemical analyses of prostate cancer xenografts grown subcutaneously in SCID mice. Asterisk indicates stroma. Original magnification, ×400.

MDA PCa 118 cells express FGF9, which induces new bone formation. To identify the mechanism underlying the induction of ectopic bone formation, we performed a differential gene array analysis to compare gene expression of the MDA PCa 118a, MDA PCa 118b, MDA PCa 2b, and PC3 cells. We chose to compare these xenografts because they were all derived from bone metastases of prostate cancer but only the MDA PCa118 xenografts could induce the ectopic formation of bone (12, 29). We have established that ectopic osteogenesis is mouse derived and probably mediated by paracrine factors produced by the prostate cancer cells. The gene expression profile indicated that *IGF1* and *FGF9* were among the most-upregulated genes ($P < 0.00015$ and $P < 0.000105$, respectively) (Supplemental Table 1), findings that we confirmed by RT-PCR (Figure 6A) and immunohistochemical staining (Figure 6B). Further tests of the effect of these factors on the growth of primary mouse osteoblasts revealed that FGF9, but not IGF1, induced osteoblast proliferation (Figure 7, A and B). Furthermore, FGF9-induced osteoblast proliferation was significantly blocked by treatment with Ab against FGF9 (Figure 7B). Similar results were obtained with the preosteoblast cell line MC3T3-E1 (data not shown). Because IGF1 and FGF9 have mitogenic effects on various cell types and have been implicated in the regulation of bone formation (30–32), we next tested whether IGF1 would enhance the effect of FGF9 on primary mouse osteoblasts. No additive effect on proliferation was found (Figure 7C). Finally, FGF9 induced new bone formation in an organ culture assay with newborn mouse calvariae (Figure 7, D–F); IGF1 did not enhance the effect of FGF9 on the formation of new bone (data not shown). Because FGF9 treatment of mouse calvariae resulted in increased osteoid but not calvaria thickness, we performed an organ culture assay for longer periods (12 days) and found that in this case, FGF9 treatment resulted in increased calvaria thickness (Supplemental Figure 3). These results indirectly implicated FGF9 in the MDA PCa 118–induced osteogenesis.

FGF9 mediates the MDA PCa 118–induced osteoblast proliferation. To clarify the contribution of FGF9 in the osteoblast proliferation induced by MDA PCa 118 cells, primary mouse osteoblasts growing alone or in coculture with MDA PCa 118b cells were treated with neutralizing Ab against FGF9 or IgG isotype (R&D Systems). We first showed that the number of osteoblasts (as assessed by thymidine incorporation into the cells' DNA) was significantly increased after coculturing with MDA PCa 118b cells ($P < 0.001$; Figure 7G). Then, in an independent coculturing experiment, we found that neutralizing Ab against FGF9 reduced the MDA PCa 118b–induced primary mouse osteoblast proliferation in a dose-dependent man-

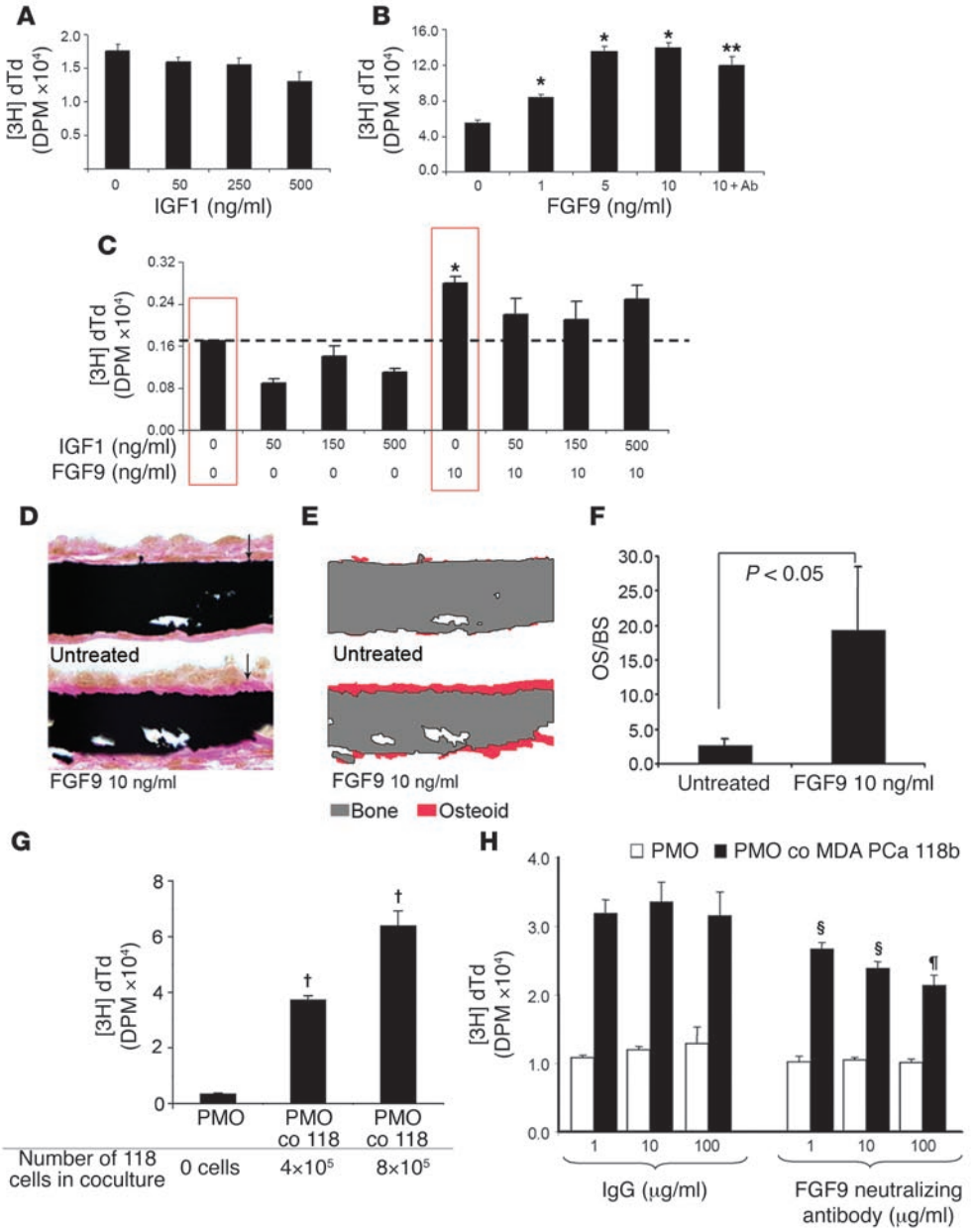

Figure 7

Effects of FGF9 on osteoblast proliferation and new bone formation. (**A**–**C**) [^{3}H]thymidine ([3H] dTd) incorporation into primary mouse osteoblasts after 48 hours of culturing in medium alone or medium supplemented with increasing concentrations of IGF1 (**A**), with increasing concentrations of FGF9 or 10 ng/ml of FGF9 plus 1 μg/ml of Ab against FGF9 (**B**), or with both (**C**). Results were confirmed in 2 independent experiments. *P < 0.01, control versus treatment; **P < 0.01, primary mouse osteoblasts cultured with 10 ng/ml of FGF9 versus primary mouse osteoblasts cultured with 10 ng/ml of FGF9 plus 1 μg/ml of Ab against FGF9. (**D**) Von Kossa–stained cross sections of bone (calvarial) organ cultures left untreated or treated with 10 ng/ml of FGF9. Each treatment condition included calvariae from 3 different mice. Arrows indicate osteoid (i.e., uncalcified bone matrix). Original magnification, ×1,000. (**E**) Schematic representation of the images in **D** illustrates the calcified bone matrix (gray) and osteoid (red) components. (**F**) Osteoid surface (OS) area versus bone surface (BS) area on the von Kossa–stained sections as quantified with the OsteoMeasure system. Similar results were obtained in another independent experiment. P < 0.05 for untreated versus FGF9-treated calvariae. (**G**) [^{3}H]thymidine incorporation into primary mouse osteoblasts growing alone (PMO) and into those cocultured with MDA PCa 118b cells (PMO co 118). Similar results were obtained in an independent experiment. †P < 0.001, PMO versus PMO co 118. (**H**) [^{3}H]thymidine incorporation into PMO or PMO co 118b and treated with 1–100 μg/ml of FGF9-neutralizing Ab or the IgG isotype control. P < 0.001, PMO versus PMO co 118b; §P < 0.05, ¶P < 0.01, PMO co 118b plus FGF9-neutralizing Ab versus PMO co 118b plus IgG. Similar results were obtained in an independent experiment. In A–C and F–H, data are presented as mean ± SEM.

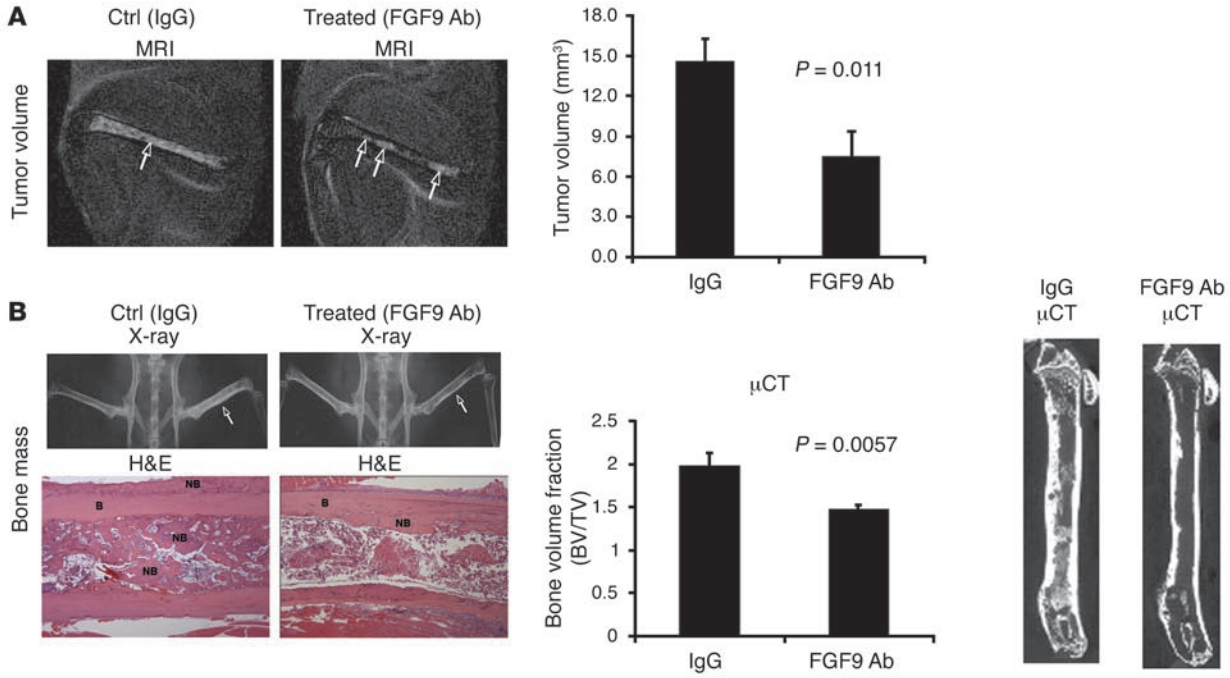

Figure 8

Effects of FGF9 blockade on MDA PCa 118b bone growth and osteoblastic reaction in vivo. (**A**) Tumor volume. MDA PCa 118b tumor visualized and quantified by T2-weighted, fat-suppressed MR. Left and middle: Representative axial MR images of mice injected with MDA PCa 118b cells in the femur and obtained after 5 weeks of treatment with FGF9-neutralizing Ab or IgG isotype. Arrows indicate tumor. Tumors were confined to the bone, spreading throughout the femur area in the IgG-treated mice (control) and scattered in the bone area in the mice treated with FGF9-neutralizing Ab. Right: Volumes of regions of increased signal in the MDA PCa 118b–injected femur measured by MR after 5 weeks of treatment were significantly higher in the control than in the treated mice ($P = 0.011$). (**B**) Bone mass. X-ray: Radiographs show mouse pelvis and rear limbs of mice 7 weeks after intrafemoral injection of MDA PCa 118b cells in the control and treatment groups. Arrows indicate area illustrated in the lower panels. H&E: H&E-stained sections of MDA PCa 118b–bearing femurs. Note that the marrow cavity is filled with new bone (NB) in the femurs of the control but not the treated mice. B, bone matrix; NB, new bone. μCT: Effect of FGF9 blockade on bone volume fraction. Bottom right: Cross-sectional μCT images of both control treated (IgG) and neutralizing Ab–treated (FGF9 Ab) tumor-bearing bones. Error bars indicate SEM.

ner ($P < 0.05$ with 1–10 μg/ml FGF9 Ab and $P < 0.01$ with 100 μg/ml FGF9 Ab; Figure 7H). IgG had no effect on the proliferation of osteoblasts alone or in coculture with MDA PCa 118b cells. Neutralizing Ab against FGF9 had no growth-inhibitory effect on osteoblasts growing alone (Figure 7H). These results suggested that FGF9 mediates MDA PCa 118b–induced osteogenesis.

Mice treated with FGF9-neutralizing Ab developed significantly smaller MDA PCa 118b bone tumors and reduced osteoblastic reaction. To assess in vivo the relevance of FGF9 in the osteoblastic bone growth of this model, we examined the effect of blocking FGF9 signals in mice injected with MDA PCa 118b cells into their femurs. MRI analysis of MDA PCa 118b tumors 5 weeks after cell injection demonstrated that the mice treated with FGF9-neutralizing Ab developed significantly smaller tumors than controls did ($P = 0.011$; Figure 8). Note that at this time point (5 weeks), tumors were confined to the bone (Figure 8), probably because we injected fewer cells (1×10^6) than in the initial experiments so that we could closely monitor tumor progression. In order to assess whether the MDA PCa 118–induced bone reaction was also affected by FGF9 blockade, we subsequently monitored the tumor-associated bone mass by weekly x-ray analysis and terminated the experiment 7 weeks after cell injection (2 weeks after the end of treatment). We then performed specimen microCT analysis (20-μm resolution) of tumor-bearing bones and found a significantly lower bone volume in the femur of treated compared with control mice ($P = 0.0057$). Accordingly, histological analysis of tumor bearing bones demonstrated widespread areas of woven bone in control but not treated femurs (Figure 8). These results suggest that FGF9 plays an important role in the osteoblastic progression of MDA PCa 118b cells in bone.

FGF9 is expressed by human prostate cancer cells but not by normal prostate epithelial cells. We then assessed expression of FGF9 in 7 normal human prostate and 82 human prostate cancer tissue specimens by immunohistochemical analysis with Ab against human FGF9 (R&D Systems). In agreement with previous reports, FGF9 was not expressed by normal prostate epithelial cells but was expressed by prostate stromal cells (33). However, we found positive FGF9 staining in prostate cancer cells in 24 of 56 primary tumors derived from organ-confined prostate cancer (Table 1). We then studied FGF9 expression in bone metastases and found that all 25 samples studied stained positive for FGF9 expression (with various staining intensities; Table 1). Figure 9 shows examples of normal prostate, 1 primary prostate cancer with negative staining, 1 primary prostate cancer with positive staining, and 2 bone metastases with positive staining. These findings were confirmed by RT-PCR analysis of RNA obtained by laser-capture microdissection of normal prostate epithelial cells and prostate cancer epithelial cells derived from 2 bone metastases from prostate cancer (Figure 9). A statistically significant correlation was found between clinical stage (primary

Table 1
Results of immunostaining for FGF9 expression in human prostate cancer tissue specimens grouped by type of lesion

Tissue	Negative	Positive (staining intensity)[A]			P
		+	++	+++	
Normal prostate (n = 7)	7 (100%)	0	0	0	
Primary prostate cancer (n = 56)	32 (57%)	22 (39%)	2 (4%)	0	
Bone metastases (n = 25)	0	3 (12%)	10 (40%)	12 (48%)	<0.0001[B]

FGF9 expression in normal prostate epithelium and prostate cancer was assessed by immunohistochemical staining with Ab against human FGF9. [A]Staining intensity was considered relative to that for MDA PCa 2b cells (negative), PC3 cells (+), and MDA PCa 118 cells (+++). [B]Fisher's exact test.

prostate cancer and bone metastases) and FGF9 expression. However, no statistically significant association between Gleason score or bone phenotype (blastic, mixed, or lytic) and FGF9 staining was found (Table 1). These results suggested that FGF9 plays a role in the progression of prostate cancer to a metastatic phenotype. The lack of association with a bone phenotype likely reflects the heterogeneity of prostate cancer bone metastases and the multifactorial nature of the interaction between prostate cancer and bone.

Discussion

We report here the successful establishment of 2 prostate cancer xenografts (MDA PCa 118a and 118b) derived from a bone metastasis in a man with castration-resistant prostate cancer. The prostate cancer cells in these xenografts, like those in the human tumor biopsy of origin, do not express androgen receptor or PSA and can grow subcutaneously in castrated mice. These results suggest that androgen receptor–null cells contribute to the development or progression of castration-resistant prostate cancer, and they agree with recent reports that androgen receptor expression on tumors varies in advanced disease (18). We also found that MDA PCa 118 xenografts induced robust osteoblastic reactions in bone, recapitulating features of the human tumor of origin. This is, to our knowledge, the first experimental evidence that androgen receptor–null cells contribute to the osteoblastic progression of castration-resistant prostate cancer in bone, and it highlights the importance of androgen receptor–independent pathways in the osteoblastic progression of prostate cancer in bone.

Ectopic bone formation can be induced experimentally by the transplantation of a variety of living cells in addition to the implantation of decalcified bone matrix (34, 35). However, to the best of our knowledge, MDA PCa 118 xenografts are the first human cancer model in which the process of ectopic osteogenesis parallels tumor growth. In other models of ectopic osteogenesis, the new bone formation is usually surpassed by a progressive tumor that has direct or indirect resorptive effects on the new bone formed (34, 35). This strong osteoinductive activity of MDA PCa 118 xenografts may reflect a unique osteogenic program typical of prostate cancer and may explain the tropism of prostate cancer cells for bone.

We also used gene expression profiling to identify several candidate mediators of MDA PCa 118–induced osteogenesis. BMPs are members of the TGF-β family that are essential for the commitment and differentiation of mesenchymal cells to the osteoblastic lineage, and they are the only known molecules that can induce the formation of bone on subcutaneous or intramuscular implantation (36, 37). BMPs have also been implicated in the formation of new bone induced by prostate cancer (38). Thus, one could speculate that BMPs mediate the ectopic osteogenesis induced by the MDA PCa 118 xenografts. However, additional osteogenic factors are likely to contribute to the strong osteoblastic phenotype seen in MDA PCa 118b. For instance, the prostate cancer cell line PC3, which expresses several *BMP* genes, induces an osteolytic reaction in bone and does not induce ectopic osteogenesis. Because the bone phenotype induced by prostate cancer cells results from a balance between proteins that induce bone formation and those that promote resorption, the biologic effect of BMPs will depend on the presence of inhibitors (e.g., Noggin) and/or bone anabolic factors that may cooperate with BMPs to mediate the new bone formation induced by MDA PCa 118 xenografts.

In addition to *BMP* genes, the MDA PCa 118 cells expressed *WNT* ligands. Wnts are a family of secreted proteins that affect various aspects of skeletal development and tumor biology and are of particular interest in bone metastasis (39, 40). Indeed, the paracrine activation of the Wnt canonical pathway has been implicated in the formation of new bone by prostate cancer (23, 24). However, MDA PCa 118 cells expressed *DKK1*, a Wnt inhibitor implicated in the pathogenesis of bone lysis from multiple myeloma (27) and suspected of blocking the effects of prostate cancer–secreted Wnt ligands on osteoblast proliferation (23, 24). Hence, the balance between DKK1 and Wnt ligands produced by MDA PCa 118 cells would probably determine whether these cells induce the paracrine activation of Wnt canonical signals in mesenchymal cells and/or osteoblasts. Finally, in accordance with the concept that prostate cancer bone metastases are fundamentally osteoblastic but often

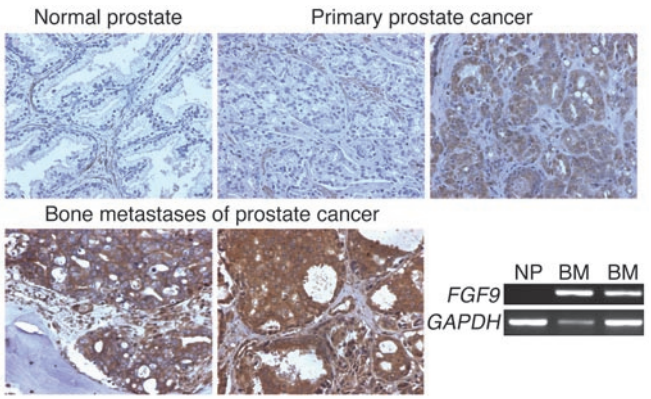

Figure 9
FGF9 expression in normal prostate and prostate cancer. Upper panels and lower left and middle panels: Immunohistochemical staining with Ab against FGF9 in normal prostate, 2 cases of organ-confined primary prostate cancer (1 positive and 1 negative for FGF9 expression), and 2 cases of bone metastases of prostate cancer. Original magnification, ×200. Lower right panel: RT-PCR analysis of *FGF9* expression in normal prostate (NP) and 2 case of bone metastases of prostate cancer (BM).

have an osteolytic component, we found that osteoclasts in the MDA PCa 118 xenografts and MDA PCa 118 cells expressed the mediator of osteoclast activation *PTHRP*.

We also found that MDA PCa 118a and MDA PCa 118b cells expressed high levels of *IGF1* and *FGF9*. Although IGFs are thought to have important roles in bone formation (41), we did not find that IGF1 affected the proliferation of osteoblasts, either by itself or in combination with FGF9. Our findings, plus those of a recent study suggesting that IGF1 does not participate in prostate cancer–induced new bone formation (42), led us to focus on FGF9. FGF9, also known as glial activating factor, is a secreted glycosylated protein that has mitogenic effects on a variety of cell types and is thought to selectively expand committed osteogenic cell populations (30, 31). FGFs bind and signal through low- and high-affinity FGF receptors (FGFRs). The high-affinity receptors for FGF9 are FGFR2 (IIIc isoform), FGFR3 (IIIb and IIIc isoforms), and FGFR4, which are structurally similar to transmembrane receptor tyrosine kinases (43). *Fgfr2IIIc*$^{-/-}$ mice show delayed ossification and decreased runt-related transcription factor 2 transcription, suggesting that FGFR2IIIc is a positive regulator of ossification that affects mainly osteoblasts (44). FGF9 was previously thought to be mitogenic for prostate epithelial cells (45), but its role in prostate cancer bone metastases has not been investigated. Our findings that MDA PCa 118 xenografts expressed FGF9, that the MDA PCa 118–induced osteoblast proliferation was blocked by FGF9 Ab, that FGF9 induced the formation of new bone in an organ culture assay, and that FGF9 blockade in vivo resulted in a reduced tumor-associated bone mass as compared with control treatment suggest that this factor is implicated in the induction of new bone by MDA PCa 118 cells. Finally, it was previously suggested that FGF9 induces the activation of mature osteoblasts and cannot activate preosteoblasts (30). Thus, FGF9 likely contributes to MDA PCa 118–induced ectopic osteogenesis by cooperating with other factors. In particular, MDA PCa 118 cells produced several BMPs, which are known to induce the commitment of mesenchymal cells to the osteoblastic lineage (36, 37). Thus, FGF9-induced proliferation of these committed osteoblasts may contribute to the process of ectopic osteogenesis, which is usually self-limiting (34, 35).

Our studies of FGF9 expression in human tissue specimens of normal prostate and prostate cancer confirmed that FGF9 was not expressed by normal prostate epithelial cells but was expressed by prostate stromal cells, as previously reported (33). However, we found positive staining for FGF9 in prostate cancer cells in 24 of 56 primary tumors derived from organ-confined prostate cancer and in all the bone metastases we studied. This switch in the source of FGF9 from the stroma to the cancer cells could increase the availability of FGF9, thereby favoring prostate cancer growth or survival at metastatic sites. Indeed, our findings that mice treated with FGF9-neutralizing Ab developed significantly smaller MDA PCa 118b tumors and reduced bone reaction compared with mice in the control group support the concept that FGF9 plays a role in prostate cancer progression and warrant further research to assess its role in the growth of prostate cancer cells in bone.

In summary, we have established a new androgen receptor–null model of prostate cancer that recapitulates the osteoblastic phenotype of prostate cancer in bone and induces ectopic osteogenesis in mice. Our studies support the concept that targeting androgen receptor–null cells will be critical in the treatment of prostate cancer bone metastases. In addition, this new osteogenic xenograft model should help us to identify signaling pathways involved in the progression of prostate cancer in bone and will be an important preclinical model for testing the effect of various treatment regimens for bone metastases.

Methods

Collection and implantation of tissue specimens into immunodeficient mice. Human tissue specimens were residual samples from diagnostic biopsies or surgery for bone metastases in 7 men with prostate cancer. Written informed consent had been obtained from patients before sample acquisition, and all samples were processed according to a protocol approved by the Institutional Review Board of the University of Texas MD Anderson Medical Center. On collection, the specimens were placed in cold (4°C), sterile α-MEM (GIBCO; Invitrogen), and small pieces were then implanted into subcutaneous pockets of 6- to 8-week-old male CB17 SCID mice (Charles River Laboratories). In some cases, several tissue samples were available from the same patient. In those cases, each tissue specimen was named as a tumor variant and implanted into a different mouse. Thus, we processed 17 bone tissue specimens obtained from 7 men with prostate cancer bone metastases. Tissue sections taken from locations immediately adjacent to the samples used for implantation were processed for histopathologic analysis. Mice were monitored weekly for tumor growth. All animal experiments were conducted in accordance with accepted standards of animal care and were approved by the Institutional Animal Care and Use Committee of the University of Texas MD Anderson Cancer Center. Serum PSA levels were measured as previously described (16).

Patient clinical history. MDA PCa 118a and MDA PCa 118b tumor lines were derived from a 49-year-old man of mixed European descent who presented with PSA blood levels of 5,200 ng/ml and widespread bone metastases. No lymph node or visceral metastases were found at that time. The disease had previously responded to hormone ablation therapy but later progressed, at which time the patient was given trastuzumab and palliative radiation therapy to a destructive lesion at the base of the skull. Over the next 4 weeks, he experienced left hemipelvic pain, a palpable mass in the left gluteal area, and a serum PSA level of 400 ng/ml. Radiologic studies revealed widespread sclerotic and lytic osseous metastases, with 2 large soft-tissue masses arising from the left hemipelvis (left ilium and pubis) and multiple liver lesions. Biopsy specimens of the soft-tissue masses and liver lesions revealed high-grade carcinoma. At that time, the patient was given weekly doses of i.v. paclitaxel (80 mg/m^2) and carboplatin (area under the curve of 2) and twice-daily doses of oral diethylstilbestrol (1 mg) and continued with twice-daily low-dose dexamethasone (0.5 mg). Within 2 months, the patient's PSA level had declined to 87 ng/ml, the pain had resolved, and his energy level had greatly improved. Follow-up imaging revealed marked regression of the liver lesions and shrinkage of the soft-tissue masses, which exhibited faint and patchy osteosclerotic or calcific appearance at the rims, dense ossification, and intense uptake of radionuclides. The patient remained on this systemic regimen for 2 months, when worsening left pubic pain and swelling led to repeat imaging. CT scans revealed an enlarging left pubic mass but a stable left iliac mass. Biopsy of the left pubic mass revealed high-grade carcinoma. After written informed consent was obtained from the patient, biopsy material from the left pubis and left ilium was used for implantation into immunodeficient mice. The patient was given palliative radiation therapy to the left hemipelvis, followed by etoposide-based chemotherapy but subsequently developed progressive generalized bone pain, cord compression, and encephalopathy followed by death. No brain metastases were identified at autopsy.

Chromosome preparation and Giemsa banding. Because MDA PCa 118b cells do not grow well in vitro, to perform karyotype analysis we directly injected tumor-bearing mice with colcemid (0.1 ml of 20-μg/ml solution, intraperitoneally). Four hours after colcemid treatment, the tumor-bearing mice were euthanized, the tumor was harvested and mechanically dissociated, and the cells were directly processed for chromosome preparation. Briefly, MDA PCa 118b cells were kept in α-MEM for 30 minutes, then

harvested using a hypotonic potassium chloride solution (0.075 M) and fixed in acetic acid/methanol (1:3 vol/vol). Slides were prepared after routine air drying. Optimally aged slides were used for Giemsa banding (46), and 5 metaphases were karyotyped in detail.

Cell cultures. MDA PCA 2b cells, developed in our laboratory (16), were propagated in BRFF-HPC1 medium (AthenaES) with 20% FBS (GIBCO; Invitrogen). PC3 cells, obtained from the ATCC, were maintained in RPMI 1640 (GIBCO; Invitrogen), and VCaP cells, a kind gift of Kenneth Pienta (University of Michigan, Ann Arbor, Michigan, USA), were maintained in DMEM, high glucose (GIBCO; Invitrogen), both supplemented with 10% FBS. For the mitogenic assays, primary cultures of murine osteoblasts were established as described elsewhere (12), and the murine preosteoblast cell line MC3T3-E1 (subclone 4) was obtained from ATCC (catalog no. CRL-2593).

Propagation of prostate cancer xenografts. Samples of the subcutaneous xenografts obtained as described above were removed at necropsy, and small pieces were directly implanted into subcutaneous pockets of 6- to 8-week-old male CB17 SCID mice (Charles River Laboratories). For the studies of tumorigenesis in male (sham-operated), female, and castrated male mice, as well as for the time-course studies, samples of the subcutaneous xenografts removed at necropsy were dissected into small clumps, mechanically dispersed, and filtered to obtain single-cell suspensions. Cells were counted using a hemacytometer, aspirated into a syringe, and injected subcutaneously into SCID mice with a 22-gauge needle (4×10^6 cells per mouse). We used 5 mice per group for the tumorigenesis studies, and tumor dimensions were measured with calipers at weeks 2, 3, 4, and 5. For the time-course studies, we used 4 mice, euthanizing 1 mouse per week (between weeks 1 and 4) and processing the harvested tumors as described below.

Histologic and immunohistochemical analyses of mouse tissues. Subcutaneous tumor samples were fixed in 4% paraformaldehyde and decalcified in formic acid as previously described (12). Serial 5-μm tissue sections were cut from each sample; one section was stained with H&E, and adjacent sections were used for immunostaining or FISH analysis as described below. Other sections were assayed for staining with TRAP (11), an enzyme specifically expressed by osteoclasts in the bone marrow. Pieces of tissue from the subcutaneous tumors were also fixed and embedded in methylmethacrylate. The undecalcified methylmethacrylate-embedded tissues were then cut in 5-μm sections with a rotation microtome (Leica) and processed for von Kossa or alkaline phosphatase staining as described previously (47–49). For the time-course studies, the undecalcified methylmethacrylate-embedded tissues were cut in 10-μm sections, mounted on slides, and stained with Alcian blue overnight. Those slides were subsequently washed in 95% ethanol, stained in alizarin red for 3 hours, washed in alcohol, cleared in xylene, and mounted.

Immunohistochemical analyses. Tissue sections were dewaxed with xylene and rehydrated in a graded series of alcohol. When recommended by the Abs' suppliers, antigens were unmasked by boiling the tissue sections in 0.01 M sodium citrate (pH 6.0) with 0.1% NP-40 for 10 minutes. All samples were then processed according to standard procedures, except for the samples to be stained for human mitochondria, which were permeabilized with 0.1% Triton X-100 in PBS for 10 minutes at room temperature. Samples were then incubated with a cocktail of 3 different Abs against cytokeratins (Ab clone Zym5.2 [Zymed Laboratories; Invitrogen], clones MNF116 and AE1/AE3 [Dako], and clone CAM 4.2 [BD]) in a single staining procedure. Samples were also incubated with Abs against vimentin (clone V9; Dako; 1:600 dilution); chromogranin A (Zymed Laboratories; Invitrogen; prediluted); synaptophysin (clone sy38, Dako; 1:200 dilution); mitochondria (clone 113-1, an Ab against the surface of intact human mitochondria; Chemicon; 1:100 dilution); androgen receptor (clone AR441; Dako; 1:30 dilution); PSA (1:3,000 dilution) and prostatic acid phosphatase (1:50 dilution; both from Dako); and IGF1 (2.5 μg/ml) and FGF9 (5 μg/ml; both from R&D Systems). Ab binding was detected with a DAB kit (Dako) in which 3,3′-diaminobenzidine was the chromogen, and the sections were then counterstained with hematoxylin.

Western blot analysis of the androgen receptor. For Western blotting, 25 μg of protein from tissue extracts was separated on 4%–20% Tris-glycine polyacrylamide gels and transferred to nitrocellulose membranes (both from Novex; Invitrogen). The androgen receptor was detected by enhanced chemiluminescence (Amersham; GE Healthcare) after incubation with primary Abs (goat polyclonal from Santa Cruz Biotechnology Inc. and rabbit polyclonal from Upstate [Millipore]), followed by incubation with the appropriate secondary Ab. We used 2 different polyclonal Abs against the androgen receptor so that we could target different epitopes.

Intrafemoral injection of xenografts. Samples of the subcutaneous xenografts were removed at necropsy, dissected into small clumps, and filtered to obtain single-cell suspensions. Cells were counted using a hemacytometer and aspirated into a syringe, and then 1.5×10^6 cells per mouse were injected with a 28-gauge needle into the distal ends of the femurs of 6- to 8-week-old intact male SCID mice according to procedures described elsewhere (12). Each xenograft variant was injected into 8 mice. The mice were euthanized with an overdose of anesthetic 9 weeks after injection, after which their hind legs were removed and the muscle tissues dissected from the bones of both the injected and control hind limbs of mice bearing the femoral xenografts. The dissected bones were then processed for histological and histomorphometric analysis.

Histomorphometric analysis of bone xenografts. Quantification of osteoblasts and osteoclasts was performed using the OsteoMeasure software system (OsteoMetrics) on tissue sections obtained from formalin-fixed, paraffin-embedded, and decalcified specimens of tumor-bearing bones. We used 20 adjacent high-magnification fields obtained from one representative 5-μm section. Osteoblast numbers and surfaces were assessed using slides stained with toluidine blue (47) and osteoclast parameters using slides stained with TRAP, an enzyme specifically expressed by osteoclasts in the bone marrow (47). The osteoblast and osteoclast parameters measured in the growth plate of the contralateral femurs of these mice were used as normal controls.

FISH analysis. For FISH, either a Cy3-labeled mouse Y chromosome paint probe (Cambio) or FITC-labeled human centromere probes for chromosome 7 (Vysis; Abbott Molecular) was used with paraffin-embedded tissue sections according to the manufacturer's protocol. The slides were counterstained with DAPI, and photomicrographs of the FISH preparations were taken with a Nikon photomicroscope equipped with filters for DAPI (UV-2a), Cy3, and FITC and with a cooled charge-coupled device camera.

Semiquantitative RT-PCR. RNA for these experiments was extracted from whole MDA PCa 118a and MDA PCa 118b tissues grown subcutaneously and from MDA PCa 2b and PC3 cell lysates. Results were subsequently confirmed using RNA obtained by laser-capture microdissection of serial sections from fresh frozen tissues of the MDA PCa 118a, MDA PCa 18b, MDA PCa 2b, and PC3 subcutaneous xenografts. Laser-capture microdissection was performed using a PixCell LCM system equipped with an infrared diode laser (Arcturus Engineering) according to published protocols (50). To prepare RNA from the laser-capture-microdissected cells, we used 2 pools of MDA PCa 118a and MDA PCa 118b xenograft cells (5,000 cells each) and 1 pool of MDA PCa 2b and PC3 xenograft cells (5,000 cells each). RNA was extracted by using a Picopure RNA isolation kit and subsequently amplified with a RiboAmp OA RNA amplification kit (both from Arcturus Engineering). Following the same procedures, we also performed laser-capture microdissection and prepared RNA from 1 pool of normal prostate epithelial cells (5,000 cells) and 2 pools of prostate cancer epithelial cells derived from 2 bone metastases from prostate cancer (5,000 cells each). For cDNA preparation, the RNA was first treated with DNase I (Invitrogen), and reverse transcription was done using Superscript II (Invitrogen) according to the manufacturer's protocol. Reverse transcription reactions were ampli-

fied by PCR with gene-specific primers (Supplemental Table 2) under standard reaction conditions. All products were resolved on 2% agarose gels.

Microarray gene expression profiling and data analysis. cDNA derived from the laser-capture-microdissected MDA PCa 118a, MDA PCa 118b, MDA PCa 2b, and PC3 subcutaneous xenografts obtained as described in the previous section was used for gene array analyses. Gene expression profiling was done at the Microarray Core Facility (MD Anderson Cancer Center). All samples were hybridized against the Affymetrix human genome U133A microarray, which contains 22,283 probes representing 12,182 unique UniGene clusters (UniGene build 185, September 2005). All array data were quantified and normalized using the DNA-Chip Analyzer 2004 version (51) (http://biosun1.harvard.edu/complab/dchip/). Gene expression measurements were logarithm transformed (base 2) for further analysis.

To identify genes expressed differently by cancer cells in the MDA PCa 118 variants and the other 2 prostate cancer xenografts, MDA PCa 2b and PC3, 2-sample *t* tests were applied as the test statistic. To adjust for multiple testing, we applied a beta-uniform mixture to model the resulting *P* values computed from the test statistic and assessed the false discovery rate to identify differently expressed genes (52). By setting the false discovery rate at less than 5% (corresponding to $P < 0.00081$) as a cutoff, we identified 248 genes (Supplemental Table 2) that were expressed differently by the 2 groups of prostate cancer cells.

Mitogenic assays. Primary mouse osteoblasts or MC3T3-E1 cells were grown in α-MEM with 10% FBS, either alone or supplemented with recombinant human IGF1, recombinant human FGF9 (R&D Systems), or both. DNA synthesis was assessed by the incorporation of [^{3}H]thymidine (NEN Life Science; PerkinElmer) into DNA. The labeled thymidine was added during the final 3 hours of a 48-hour culture, and its incorporation was measured as described elsewhere (53).

Organ culture bone formation assay. Bone formation was assessed as described previously (54). Briefly, calvariae from 4-day-old CD1 mouse pups (Charles River Laboratories) were excised, cut in half, and cultured for 7 days in 6-well plates. Half of each calvaria was placed in BGJ medium (Sigma-Aldrich) containing 0.1% BSA, 50 ng/ml of heparin sulfate proteoglycan (Sigma-Aldrich), and 10 ng/ml of recombinant human FGF9 (R&D Systems). The other half of each calvaria was placed in BGJ medium containing 0.1% BSA plus 50 ng/ml of heparin sulfate proteoglycan and used as a control. Each half-calvaria was placed on a cell culture insert that suspends the bone organ between atmosphere and medium for optimal CO_2 exchange. The medium was changed every 2 days, and the experiment was terminated after 7 days. At the end of the cultures, the calvaria halves were fixed in formalin, embedded in methylmethacrylate, sectioned, stained with von Kossa reagent, and photographed with a high-resolution video camera (Sony 3CCD) linked to a Nikon microscope. The OsteoMeasure software system (OsteoMetrics) was used to estimate the osteoid surface area of the calvaria sections. Measurements on all samples were taken approximately 160 μm from the frontal suture of the calvaria for a distance of 2 mm. The osteoid covering the bone was measured first, followed by the total bone surface, and the degree of bone surface covered by osteoid was expressed as the ratio of osteoid surface area to bone surface area.

Coculture studies. Tumor areas of the subcutaneous MDA PCa 118b xenografts removed at necropsy were mechanically disaggregated into single-cell suspensions, filtered, and counted using a hemocytometer. Cells were then plated in cell culture dishes and grown in α-MEM with 10% FBS for 24 hours. We subsequently cocultured MDA PCa 118b cells with primary mouse osteoblasts in a bicompartmental system in which the 2 cell types share medium but are not in physical contact (12). Primary mouse osteoblasts growing alone were used as controls. Cultures and cocultures were performed using α-MEM with 2% FBS alone, with FGF9-neutralizing Ab (clone 36912; R&D Systems), or with the mouse IgG2A isotype control (R&D Systems) as indicated. After 48-hour coculturing, the numbers of primary mouse osteoblasts were estimated using a mitogenic assay, as described above.

Treatment of MDA PCa 118b tumor–bearing mice with FGF9-neutralizing Ab and monitoring of tumor volume and bone response. MDA PCa 118b (1×10^6) cells were injected into the femurs of 20 male SCID mice. In this experimental design, we injected fewer cells (1×10^6) than in the initial experiments to closely monitor tumor progression. Ten mice were treated with neutralizing Ab against FGF9 (250 μg/mouse; clone 36912; R&D Systems) i.v. twice weekly, and another 10 mice were treated with IgG isotype (250 μg/mouse; R&D Systems) i.v. twice weekly. Treatment with Ab started at the same day of cell injection and was performed for 5 consecutive weeks, at which time the tumor volumes in the femurs were determined by MRI analysis following established procedures (55). Mice were subsequently monitored for 2 more weeks, and bone formation was assessed by x-ray analysis. The experiment was then terminated at week 7, and the femurs bearing MDA PCa 118b tumors were fixed in ethanol and subjected to specimen microCT analysis to assess bone mass. Fixed specimens were subsequently decalcified, paraffin embedded, and then subjected to histopathologic analysis. MicroCT analysis was performed in the Small Animal Imaging Facility at the MD Anderson Cancer Center with a GE Enhanced Vision Systems hybrid scanner using a resolution of 20 μm. MicroView version 2.2 software (GE Healthcare) was used to calculate bone mass, and the same total volume was used (arbitrary but large enough to fit every scan) for every analysis (total volume). The software was then used to determine the total bone content for every sample. Using the same threshold (26% of the maximum), only the bone content for femur bones was measured. This bone content was then divided by the total volume value used (total volume) to obtain the bone volume/total volume ratio.

Origin and immunohistochemical analyses of human prostate, prostate cancer, and bone metastasis specimens. We used 7 samples of normal prostate tissue obtained from nontumorous areas of prostatectomy specimens. Another 56 samples of prostate cancer (8, Gleason score 6; 24, Gleason 7; 13, Gleason 8; and 11, Gleason 9) were derived from radical prostatectomy specimens from patients with organ-confined disease with no prior therapy. Another 25 samples of bone metastases were obtained from patients with prostate cancer; 4 of those patients had not received any systemic therapy for the prostate cancer, and the other 21 had experienced a relapse after androgen deprivation therapy. Among those 21 patients with androgen-independent prostate cancer, 4 had undergone only androgen deprivation therapy, and 17 had undergone androgen deprivation therapy plus chemotherapy. Radiologic evaluation of the bony areas of the specimens demonstrated that 9 samples were osteoblastic, 9 were of mixed type, and 4 were osteolytic. No radiological reports were available for 3 patients. All of these samples were selected from a tissue bank supported by the Prostate Cancer Specialized Program of Research Excellence at the MD Anderson Cancer Center. All sections were from formalin-fixed, paraffin-embedded tissue specimens; sections derived from bone metastases were decalcified in formic acid during the fixation-and-embedding process as previously described (12). After Ab titration for human specimens, the samples were stained with 20 μg/ml of FGF9 (R&D Systems) as described above. Slides were read independently by 2 investigators and classified according to staining intensity (0 or + to +++), with 0 being the least-intense staining and +++ the most-intense staining. Evaluations were concordant in 90% of the readings; differences were resolved by consensus after joint review.

Statistics. For the tumorigenesis studies in castrated male mice, female mice, and sham-operated male mice, ANOVA (with Tukey simultaneous 95% confidence intervals) and pairwise comparisons were used. For analysis of mitogenic assay results and bone formation variables in the organ culture assays, we used 2-sample *t* tests. *P* values of less than 0.05 were considered statistically significant. Fisher's exact tests and χ^2 tests were used, as appro-

priate, to evaluate the association between FGF9 expression and Gleason score, clinical stage, or type of bone lesion (blastic, mixed, or lytic).

Acknowledgments

We thank Dong Fang Yu for technical assistance in the i.v. injection of FGF9-neutralizing Ab into mice; the McDonnell laboratory for laser capture microdissection and cDNA preparation; K. Pienta (University of Michigan) for the prostate cancer cell line VCaP; C.F. Wogan for editing the manuscript; and the Bone Disease Program of Texas for supporting the Bone Histomorphometry Core Laboratory at the MD Anderson Cancer Center. This work was supported by grants from the NIH (R01 CA096797, P50 CA090270, and R01 CA111749) and the Prostate Cancer Foundation.

Received for publication June 25, 2007, and accepted in revised form June 4, 2008.

Address correspondence to: Nora M. Navone, Department of Genitourinary Medical Oncology, Unit 1374, The University of Texas MD Anderson Cancer Center, 1515 Holcombe Boulevard, T7.3920, Houston, Texas 77030-4009, USA. Phone: (713) 563-7273; Fax: (713) 745-9880; E-mail: nnavone@mdanderson.org.

1. Jemal, A., et al. 2007. Cancer statistics, 2007. *CA Cancer J. Clin.* **57**:43–66.
2. Catalona, W.J. 1994. Management of Cancer of the Prostate. *N. Engl. J. Med.* **331**:996–1004.
3. Cook, G.B., and Watson, F.R. 1968. Events in the natural history of prostate cancer: using salvage curves, mean age distributions and contingency coefficients. *J. Urol.* **99**:87–96.
4. Clarke, N.W., McClure, J., and George, N.I. 1993. Osteoblast function and osteomalacia in metastatic prostate cancer. *Eur. Urol.* **24**:286–290.
5. Charhon, S.A., et al. 1983. Histomorphometric analysis of sclerotic bone metastases from prostatic carcinoma with special reference to osteomalacia. *Cancer.* **51**:918–924.
6. Edwards, J., and Bartlett, J.M.S. 2005. The androgen receptor and signal-transduction pathways in hormone-refractory prostate cancer. Part 1: modifications to the androgen receptor. *BJU Int.* **95**:1320–1326.
7. Pienta, K.J., and Bradley, D. 2006. Mechanisms underlying the development of androgen-independent prostate cancer. *Clin. Cancer Res.* **12**:1665–1671.
8. Burd, C.J., Morey, L.M., and Knudsen, K.E. 2006. Androgen receptor corepressors and prostate cancer. *Endocr. Relat. Cancer.* **13**:979–994.
9. Chen, C.D., et al. 2004. Molecular determinants of resistance to antiandrogen therapy. *Nat. Med.* **10**:33–39.
10. Corey, E., et al. 2002. Establishment and characterization of osseous prostate cancer models: Intratibial injection of human prostate cancer cells. *Prostate.* **52**:20–33.
11. Lee, Y.-P., et al. 2002. Use of Zoledronate to treat osteoblastic versus osteolytic lesions in a severe-combined-immunodeficient mouse model. *Cancer Res.* **62**:5564–5570.
12. Yang, J., et al. 2001. Prostate cancer cells induce osteoblast differentiation through a Cbfa1-dependent pathway. *Cancer Res.* **61**:5652–5659.
13. Thalmann, G.N., et al. 2000. LNCaP progression model of human prostate cancer: Androgen-independence and osseous metastasis. *Prostate.* **44**:91–103.
14. Doherty, A., Smith, G., Banks, L., Christmas, T., and Epstein, R.J. 1999. Correlation of the osteoblastic phenotype with prostate-specific antigen expression in metastatic prostate cancer: implications for paracrine growth. *J. Pathol.* **188**:278–281.
15. Nadiminty, N., et al. 2006. Prostate-specific antigen modulates genes involved in bone remodeling and induces osteoblast differentiation of human osteosarcoma cell line SaOS-2. *Clin. Cancer Res.* **12**:1420–1430.
16. Navone, N.M., et al. 1997. Establishment of two human prostate cancer cell lines derived from a single bone metastasis. *Clin. Cancer Res.* **3**:2493–2500.
17. Navone, N.M., Logothetis, C.J., von Eschenbach, A.C., and Troncoso, P. 1998. Model systems of prostate cancer: uses and limitations. *Cancer Metastasis Rev.* **17**:361–371.
18. Shah, R.B., et al. 2004. Androgen-independent prostate cancer is a heterogeneous group of diseases: lessons from a rapid autopsy program. *Cancer Res.* **64**:9209–9216.
19. Harris, S.E., et al. 1994. Expression of bone morphogenetic protein messenger RNAs by normal rat and human prostate and prostate cancer cells. *Prostate.* **24**:204–211.
20. Autzen, P., et al. 1998. Bone morphogenetic protein 6 in skeletal metastases from prostate cancer and other common human malignancies. *Br. J. Cancer.* **78**:1219–1223.
21. Masuda, H., et al. 2003. Increased expression of bone morphogenetic protein-7 in bone metastatic prostate cancer. *Prostate.* **54**:268–274.
22. Feeley, B.T., et al. 2005. Influence of BMPs on the formation of osteoblastic lesions in metastatic prostate cancer. *J. Bone Miner. Res.* **20**:2189–2199.
23. Hall, C.L., Bafico, A., Dai, J., Aaronson, S.A., and Keller, E.T. 2005. Prostate cancer cells promote osteoblastic bone metastases through Wnts. *Cancer Res.* **65**:7554–7560.
24. Li, Z.G., et al. 2008. Low density lipoprotein receptor–related protein 5 (LRP5) mediates the prostate cancer–induced formation of new bone. *Oncogene.* **27**:596–603.
25. Nelson, J.B., et al. 1995. Identification of endothelin-1 in the pathophysiology of metastatic adenocarcinoma of the prostate. *Nat. Med.* **1**:944–949.
26. Fedi, P., et al. 1999. Isolation and biochemical characterization of the human Dkk-1 homologue, a novel inhibitor of mammalian Wnt signaling. *J. Biol. Chem.* **274**:19465–19472.
27. Tian, E., et al. 2003. The role of the Wnt-signaling antagonist DKK1 in the development of osteolytic lesions in multiple myeloma. *N. Engl. J. Med.* **349**:2483–2494.
28. Mundy, G.R. 2002. Metastasis to bone: causes, consequences and therapeutic opportunities. *Nat. Rev. Cancer.* **2**:584–593.
29. Fizazi, K., et al. 2003. Prostate cancer cells-osteoblast interaction shifts expression of growth/survival-related genes in prostate cancer and reduces expression of osteoprotegerin in osteoblasts. *Clin. Cancer Res.* **9**:2587–2597.
30. Fakhry, A., et al. 2005. Effects of FGF-2/-9 in calvarial bone cell cultures: differentiation stage-dependent mitogenic effect, inverse regulation of BMP-2 and noggin, and enhancement of osteogenic potential. *Bone.* **36**:254–266.
31. Jackson, R.A., Nurcombe, V., and Cool, S.M. 2006. Coordinated fibroblast growth factor and heparan sulfate regulation of osteogenesis. *Gene.* **379**:79–91.
32. Cohen, P. 2006. Overview of the IGF-I system. *Horm. Res.* **65**:3–8.
33. Kwabi-Addo, B., Ozen, M., and Ittmann, M. 2004. The role of fibroblast growth factors and their receptors in prostate cancer. *Endocr. Relat. Cancer.* **11**:709–724.
34. Izbicka, E., et al. 1997. Effects of human tumor cell lines on local new bone formation in vivo. *Calcif. Tissue Int.* **60**:210–215.
35. Wlodarski, K.H. 1985. Orthotopic and ectopic chondrogenesis and osteogenesis mediated by neoplastic cells. *Clin. Orthop. Relat. Res.* **200**:248–265.
36. Chen, D., Zhao, M., and Mundy, G.R. 2004. Bone morphogenetic proteins. *Growth Factors.* **22**:233–241.
37. Wozney, J.M., and Rosen, V. 1998. Bone morphogenetic protein and bone morphogenetic protein gene family in bone formation and repair. *Clin. Orthop. Relat. Res.* **346**:26–37.
38. Logothetis, C.J., and Lin, S.-H. 2005. Osteoblasts in prostate cancer metastasis to bone. *Nat. Rev. Cancer.* **5**:21–28.
39. van Es, J.H., Barker, N., and Clevers, H. 2003. You Wnt some, you lose some: oncogenes in the Wnt signaling pathway. *Curr. Opin. Genet. Dev.* **13**:28–33.
40. Westendorf, J.J., Kahler, R.A., and Schroeder, T.M. 2004. Wnt signaling in osteoblasts and bone diseases. *Gene.* **341**:19–39.
41. Renehan, A.G., et al. 2004. Insulin-like growth factor (IGF)-I, IGF binding protein-3, and cancer risk: systematic review and meta-regression analysis. *Lancet.* **363**:1346–1353.
42. Rubin, J., et al. 2006. IGF-I secretion by prostate carcinoma cells does not alter tumor-bone cell interactions in vitro or in vivo. *Prostate.* **66**:789–800.
43. Ornitz, D., and Itoh, N. 2001. Fibroblast growth factors. *Genome Biol.* **2**:reviews3005.1–reviews3005.12.
44. Eswarakumar, V.P., et al. 2002. The IIIc alternative of Fgfr2 is a positive regulator of bone formation. *Development.* **129**:3783–3793.
45. Giri, D., Ropiquet, F., and Ittmann, M. 1999. FGF9 is an autocrine and paracrine prostatic growth factor expressed by prostatic stromal cells. *J. Cell. Physiol.* **180**:53–60.
46. Pathak, S. 1976. Chromosome banding techniques. *J. Reprod. Med.* **17**:25–28.
47. Baron, R., Vignery, A., Neff, L., Silverglate, A., and Santa Maria, A. 1983. Processing of undecalcified bone specimens for bone histomorphometry. In *Bone histomorphometry: techniques and interpretation*. R.R. Recker, editor. CRC Press. Boca Raton, Florida, USA. 13–35.
48. Miao, D., and Scutt, A. 2002. Histochemical localization of alkaline phosphatase activity in decalcified bone and cartilage. *J. Histochem. Cytochem.* **50**:333–340.
49. Lian, J.B., et al. 2003. Runx1/AML1 hematopoietic transcription factor contributes to skeletal development in vivo. *J. Cell. Physiol.* **196**:301–311.
50. Cho-Vega, J.H., et al. 2005. Combined laser capture microdissection and serial analysis of gene expression from human tissue samples. *Mod. Pathol.* **18**:577–584.
51. Li, C., and Wong, W.H. 2001. Model-based analysis of oligonucleotide arrays: expression index computation and outlier detection. *Proc. Natl. Acad. Sci. U. S. A.* **98**:31–36.
52. Benjamini, Y., and Hochberg, Y. 1995. Controlling the false discovery rate: a practical and powerful approach to multiple testing. *Journal of the Royal Statistical Society. Series B.* **57**:289–300.
53. Freshney, R.I. 1994. *Culture of animal cells. A manual of basic techniques*. Wiley-Liss Inc. New York, New York, USA. 486 pp.
54. Garrett, R. 2003. Assessing bone formation using mouse calvarial organ cultures. In *Bone research protocols*. M.H. Helfrich, and S.H. Ralston, editors. Humana Press. Totowa, New Jersey, USA. 183–198.
55. Kundra, V., et al. 2007. In vivo imaging of prostate cancer involving bone in a mouse model. *Prostate.* **67**:50–60.